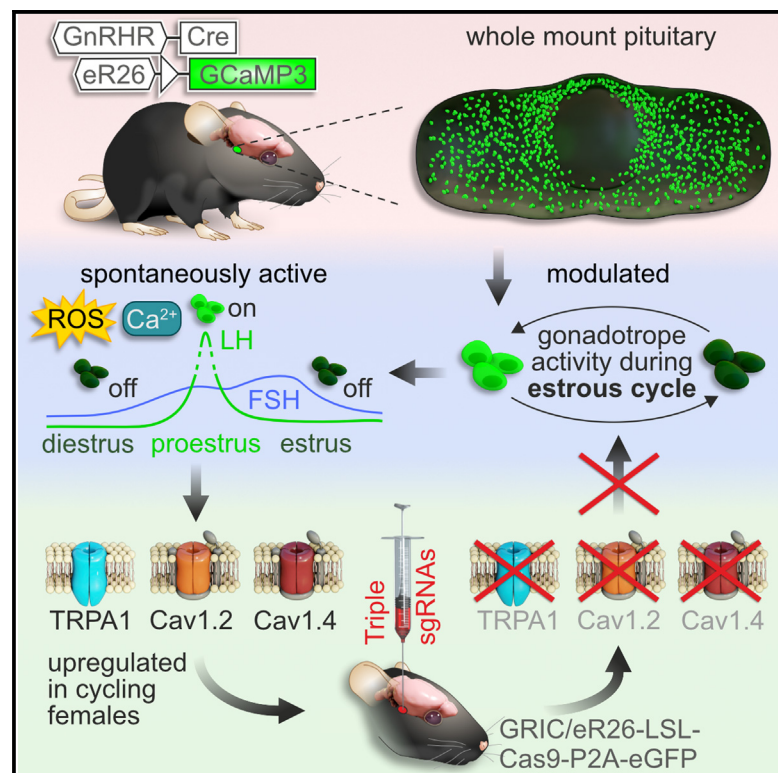# Ovulation is triggered by a cyclical modulation of gonadotropes into a hyperexcitable state

Graphical abstract

Authors

Viktoria Götz, Sen Qiao, Debajyoti Das, ..., Patrice Mollard, Michael Candlish, Ulrich Boehm

Correspondence

ulrich.boehm@uks.eu

In brief

To trigger ovulation, gonadotropes in the pituitary gland release massive amounts of luteinizing hormone (LH). Götz et al. describe a state of gonadotrope hyperexcitability during the LH surge. This is due to cyclical changes in their ion channel repertoire preceding the surge; these changes alter calcium and ROS signals in gonadotropes.

Highlights

- Female gonadotropes exhibit a state of hyperexcitability during the LH surge

- Gonadotropes cyclically change their ion channel repertoire before the LH surge

- Gonadotrope hyperexcitability depends on L-type Ca^{2+} channels and TRPA1

- Intracellular calcium and ROS signals ensure the hyperexcitable state

CelPress

Cell Reports

Report

Ovulation is triggered by a cyclical modulation of gonadotropes into a hyperexcitable state

Viktoria Götz,[1,7,8] Sen Qiao,[1,7] Debajyoti Das,[1,7] Philipp Wartenberg,[1] Amanda Wyatt,[1] Vanessa Wahl,[1] Igor Gamayun,[1] Samer Alasmi,[1] Claudia Fecher-Trost,[1] Markus R. Meyer,[1] Roland Rad,[2] Thorsten Kaltenbacher,[2] Kathrin Kattler,[3] Peter Lipp,[4] Ute Becherer,[5] Patrice Mollard,[6] Michael Candlish,[1,9] and Ulrich Boehm[1,10,*]

[1]Institute of Experimental and Clinical Pharmacology and Toxicology, Center for Molecular Signaling (PZMS), Saarland University School of Medicine, Homburg 66421, Germany
[2]Institute of Molecular Oncology and Functional Genomics, School of Medicine, Technical University of Munich, Munich 80333, Germany
[3]Department of Genetics and Epigenetics, Saarland University, Saarbrücken 66123, Germany
[4]Molecular Cell Biology, Center for Molecular Signaling (PZMS), Saarland University School of Medicine, Homburg 66421, Germany
[5]Cellular Neurophysiology, Center for Integrative Physiology and Molecular Medicine (CIPMM), Saarland University School of Medicine, Homburg 66421, Germany
[6]IGF, CNRS, INSERM, University of Montpellier, Montpellier 34090, France
[7]These authors contributed equally
[8]Present address: Institute of Pharmacology and Toxicology, University Hospital, University of Bonn, Bonn 53127, Germany
[9]Present address: Institute of Cell Biology and Neuroscience, Buchmann Institute for Molecular Life Sciences, Goethe University Frankfurt, Frankfurt am Main 60323, Germany
[10]Lead contact
*Correspondence: ulrich.boehm@uks.eu
https://doi.org/10.1016/j.celrep.2023.112543

SUMMARY

Gonadotropes in the anterior pituitary gland are essential for fertility and provide a functional link between the brain and the gonads. To trigger ovulation, gonadotrope cells release massive amounts of luteinizing hormone (LH). The mechanism underlying this remains unclear. Here, we utilize a mouse model expressing a genetically encoded Ca^{2+} indicator exclusively in gonadotropes to dissect this mechanism in intact pituitaries. We demonstrate that female gonadotropes exclusively exhibit a state of hyperexcitability during the LH surge, resulting in spontaneous $[Ca^{2+}]_i$ transients in these cells, which persist in the absence of any *in vivo* hormonal signals. L-type Ca^{2+} channels and transient receptor potential channel A1 (TRPA1) together with intracellular reactive oxygen species (ROS) levels ensure this state of hyperexcitability. Consistent with this, virus-assisted triple knockout of *Trpa1* and L-type Ca^{2+} subunits in gonadotropes leads to vaginal closure in cycling females. Our data provide insight into molecular mechanisms required for ovulation and reproductive success in mammals.

INTRODUCTION

Ovulation depends on a precisely timed release of massive amounts of luteinizing hormone (LH)[1,2] that occurs only once during the female reproductive cycle. This massive release of LH (known as the LH surge) is essential to drive oocyte maturation and, subsequently, release of the oocyte. A specialized population of cells within the anterior pituitary gland, the gonadotropes, are the source of LH. These cells are an essential component of the reproductive hypothalamic-pituitary-gonadal (hpg) axis[3] and integrate neuroendocrine and steroid hormone signals originating from the brain and the gonads, respectively.[4] Gonadotropes respond to the pulsatile release of hypothalamic gonadotropin-releasing hormone (GnRH) with an increase in $[Ca^{2+}]_i$[5] and subsequent release of gonadotropins, LH, and follicle-stimulating hormone (FSH), which control both the production of sex hormones and gametes. In females, LH and FSH elicit strict control over the ovarian cycle,[6] maintaining a 24- to 31-day

cycle[7] in humans and a 4- to 6-day cycle in rodents.[8] To do this, gonadotropes need to decode GnRH pulses differing in frequency and amplitude as well as cyclically changing steroid hormone levels to adapt LH and FSH production and release accordingly. Despite a wealth of studies analyzing how gonadotropes adapt LH and FSH release in response to GnRH,[9–12] very few experiments have examined how the gonadotropes themselves adapt to the changing physiological requirements of the reproductive cycle. Recent work has described profound transcriptional changes within gonadotropes during the estrous cycle,[13,14] yet most experiments studying these cells have been conducted in dissociated pituitary cells[15–17] or in cell lines.[18,19] Therefore, these studies on gonadotropes may have negated any influence of the reproductive cycle and, in addition, cell-to-cell communication within the anterior pituitary gland.[20]

Genetic labeling of gonadotropes in mice[21] has provided an entry toward studying the gonadotrope cell population *in situ*. To analyze $[Ca^{2+}]_i$ signals in gonadotropes, we employed a binary
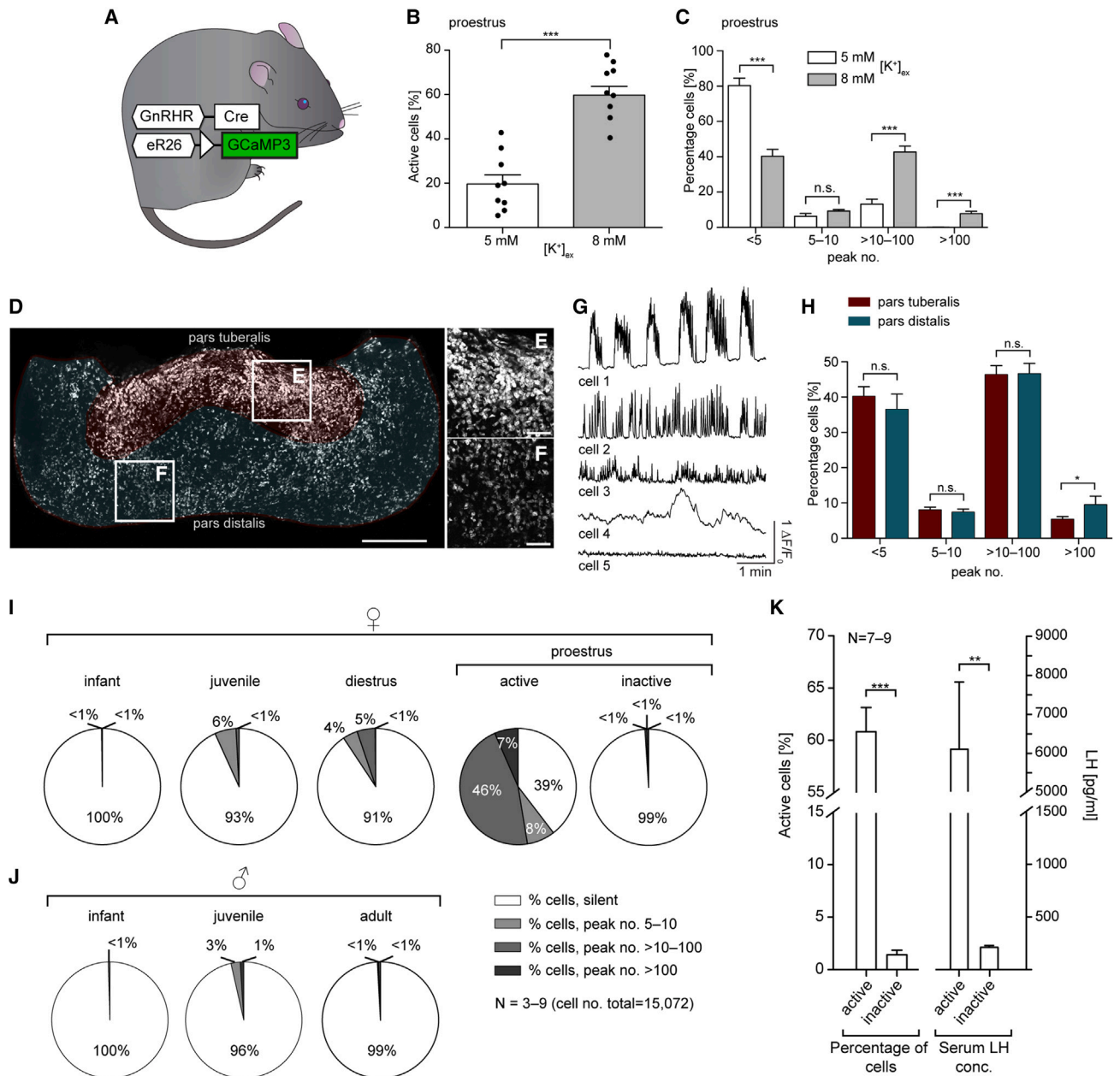
Figure 1. Unmasking gonadotrope excitability using increased $[K^+]_{ex}$ reveals that gonadotropes from a subset of proestrus females featuring spontaneous activity are hyperexcitable

(A) Genetic strategy to express GCaMP3 in gonadotropes.

(B) Cell percentage displaying spontaneous Ca^{2+} peaks (active cell ≥ 5 peaks/5 min) in 5 or 8 mM $[K^+]_{ex}$. Three different regions (black dots) were analyzed per pituitary (5 mM $[K^+]_{ex}$ $N_{mice} = 3$, $n_{cells} = 910$ vs. 8 mM $[K^+]_{ex}$ $N_{mice} = 3$, $n_{cells} = 860$; ***$p < 0.0001$).

(C) Cell percentage displaying <5 (***$p < 0.0001$), 5–10 ($p = 0.1132$), >10–100 (***$p < 0.0001$), or >100 (***$p < 0.0001$) peaks/5 min in 5 mM or 8 mM $[K^+]_{ex}$.

(D) Confocal tile- and z stack whole-mount pituitary image from a GRIC/eR26-GCaMP3 proestrus female (ventral side) displayed as maximum intensity projection.

(E and F) High magnification confocal images of the areas highlighted in (D). Scale bars, 500 μm (D), 100 μm (E and F).

(G) Representative spontaneous Ca^{2+} transients in proestrus gonadotropes. Burst-like activity (cell 1), Ca^{2+} transients with higher (cell 2) or lower amplitude (cell 3), irregular Ca^{2+} transients (cell 4), or no change in Ca^{2+} activity (cell 5) shown.

(H) Ca^{2+} transient comparison in *pars tuberalis* (red) and *pars distalis* (blue) occurring over a 5-min period. Cell groups based on peak number/5 min (<5 peaks, $p = 0.4872$; 5–10 peaks, $p = 0.6415$; >10–100 peaks, $p = 0.9598$; and >100 peaks, $p = 0.036$). Bar charts in (B), (C), and (H) are plotted with mean ± SEM.

genetic strategy to express the Ca^{2+} indicator GCaMP3 specifically in these cells.[13] We analyzed $[Ca^{2+}]_i$ signals within the gonadotrope cell population in whole-mount pituitary preparations at different reproductive cycle stages. We demonstrate that female gonadotropes display spontaneous $[Ca^{2+}]_i$ transients at the time of the LH surge. This spontaneous $[Ca^{2+}]_i$ activity persists in the absence of *in vivo* hormonal signals and GnRH signaling. Furthermore, we reveal that L-type Ca^{2+} channels and transient receptor potential (TRP) channel A1 ensure this state of hyperexcitability. Consistent with this, even partial loss of L-type Ca^{2+} channels and TRPA1 from the gonadotrope population is sufficient to perturb reproductive function in female mice. We demonstrate that alterations in intracellular ROS levels as a result of channel composition changes are important in producing this hyperexcitability. Taken together, our data show how gonadotropes are modulated during the mammalian reproductive cycle and provide mechanistic insight into the control of ovulation.

RESULTS

Gonadotropes change into a hyperexcitable state prior to ovulation

We first asked whether gonadotropes within the intact pituitary might display intrinsic $[Ca^{2+}]_i$ activity at proestrus despite the absence of GnRH signaling. Using a mouse model that expresses GCaMP3 exclusively in gonadotropes (Figure 1A), we found that ~20% (19.61% ± 4.16%; N_{mice} = 3, n_{cells} = 910) of gonadotropes were spontaneously active in whole-mount pituitary preparations from these animals. Intriguingly, however, only some pituitaries isolated from proestrus females showed these spontaneous $[Ca^{2+}]_i$ oscillations. We next asked whether the remaining ~80% of inactive gonadotropes might actually reside in a readily excitable state in these active pituitaries. To test this hypothesis, we exposed the pituitaries to slightly depolarizing conditions by increasing $[K^+]_{ex}$ from 5 to 8 mM. We found that 59.74% ± 3.98% (N_{mice} = 3, n_{cells} = 860) of gonadotropes became spontaneously active under these conditions (Figures 1B and 1C). This spontaneous activity was largely independent of the spatial position within the gland (Figures 1D–1H). These data demonstrate that the majority of gonadotropes from these females reside in a readily excitable state.

We next tested whether this state of hyperexcitability is specific to particular proestrus females or whether slightly depolarized (i.e., 8 mM KCl in artificial cerebrospinal fluid [ACSF]) conditions could also unmask spontaneous $[Ca^{2+}]_i$ oscillations in females from other developmental and estrous cycle stages (Figure S1). Strikingly, gonadotropes from infant females (N_{mice} = 5, n_{cells} = 2,353) showed no spontaneous activity (Figure 1I). Furthermore, the percentage of gonadotropes with low levels (5–10 peaks/5 min; Figure S2) of spontaneous activity was only

6% in juveniles (N_{mice} = 4, n_{cells} = 1,486) and 4% in adult females at diestrus (N_{mice} = 6, n_{cells} = 1,664). Taken together, even under slightly depolarizing conditions, spontaneous activity rarely exceeded ~10% in any developmental or estrous cycle stage except proestrus.

To determine whether this state of hyperexcitability was specific to females, we next analyzed spontaneous $[Ca^{2+}]_i$ activity in male mice in the presence of 8 mM $[K^+]_{ex}$. Spontaneous $[Ca^{2+}]_i$ activity was virtually absent in all male stages analyzed (N_{mice} = 3, n_{cells} = 1,116 for infants; N_{mice} = 6, n_{cells} = 1,384 for juveniles; N_{mice} = 5, n_{cells} = 1,311 for adults); <1% cells displayed moderate (peak no. >10–100/5 min) or high (peak no. >100/5 min) $[Ca^{2+}]_i$ activity (Figure 1J). These data demonstrate that this phenomenon occurs exclusively in female mice and only at proestrus.
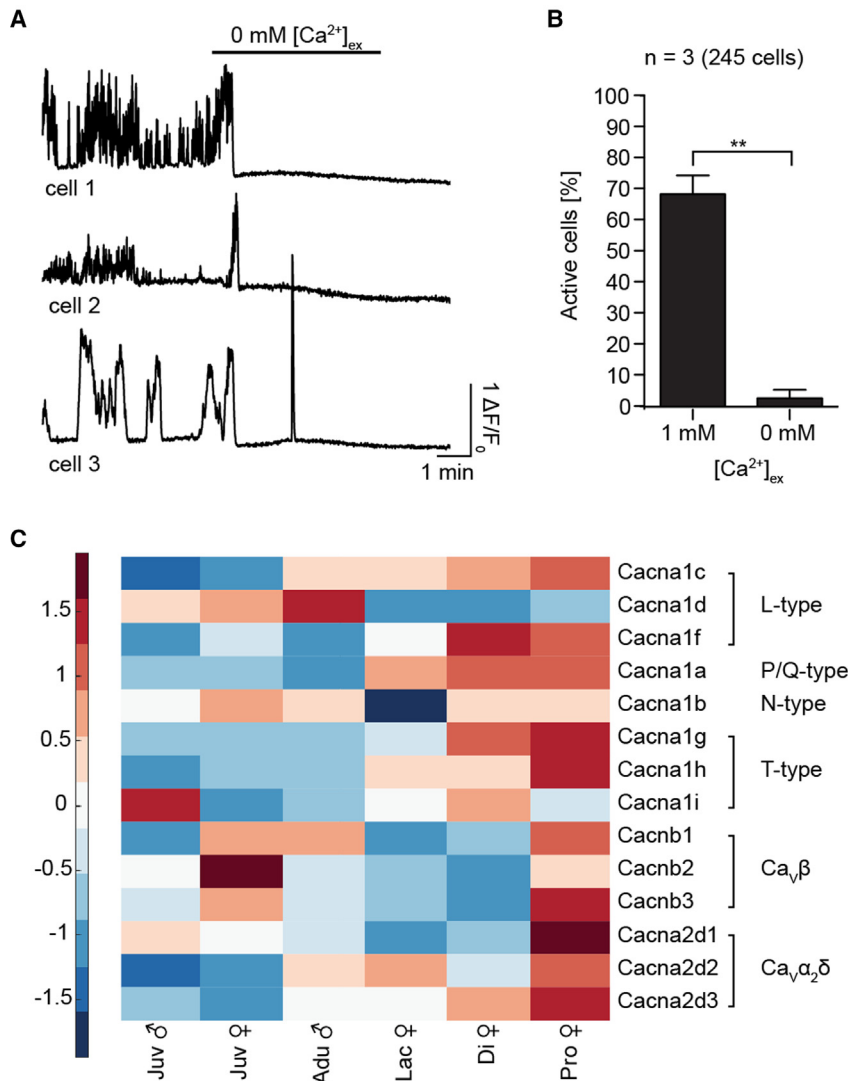
We hypothesized that gonadotrope hyperexcitability might coincide with the preovulatory LH surge at proestrus. Therefore, we analyzed proestrus females 2.5–0.5 h before the dark phase (previously, we demonstrated that LH levels in mice are likely to peak within this time window[22]) and collected trunk blood in order to correlate spontaneous $[Ca^{2+}]_i$ activity with serum gonadotropin levels. Spontaneous activity (in the presence of 8 mM $[K^+]_{ex}$) in proestrus gonadotropes showed a bimodal distribution (Figure 1I). Gonadotropes within a subset of pituitaries were highly active (Figures 1I and 1K, proestrus active), with 46% of the gonadotrope population displaying moderate and 7% high levels of spontaneous $[Ca^{2+}]_i$ activity in these preparations (N_{mice} = 8, n_{cells} = 2,937). Strikingly, LH serum levels were dramatically elevated in these animals (Figure 1K). In contrast, the remaining proestrus pituitaries (N_{mice} = 9, n_{cells} = 2,821) did not contain spontaneously active gonadotropes (Figure 1K, proestrus inactive) and were rather similar to pituitaries prepared from infant or juvenile males and females or adult males. In fact, these *inactive* proestrus pituitaries contained even lower-numbers of active gonadotrope cells than diestrus pituitaries (diestrus, 9.13% ± 2.45% vs. proestrus inactive, 1.42% ± 0.43%). Remarkably, we found that LH levels in animals with active gonadotropes were ~30 times higher (proestrus active, 6,093 ± 1,722 pg/mL; N_{mice} = 7) than those in the proestrus stage with inactive gonadotropes (proestrus inactive, 204.5 ± 17.54 pg/mL; N_{mice} = 9). FSH levels were ~3-fold higher in the animals with inactive pituitaries (786.7 ± 124.5 pg/mL, N_{mice} = 10) compared with diestrus females (277.1 ± 55.02 pg/mL, N_{mice} = 6), suggesting that these animals have already passed the LH surge and have entered estrus. Previous studies have shown that FSH levels are increased 2- to 3-fold during estrus compared with diestrus.[23] To further delineate the connection between the LH surge and spontaneously active gonadotropes at proestrus, we performed a time-dependent characterization of proestrus mice 4.5, 2.5, and 0.5 h prior to the dark phase of the light cycle. At these time points, we sacrificed the animals

(I) Cell percentage displaying spontaneous $[Ca^{2+}]_i$ peaks in different developmental and reproductive stages. Proestrus females are divided into two stages based on spontaneous $[Ca^{2+}]_i$ activity (Pro active or Pro inactive).

(J) Cell percentage displaying spontaneous $[Ca^{2+}]_i$ peaks in males in different developmental stages. Pie charts for each stage define percentage of silent cells (silent cell <5 peaks/5 min; white), cells displaying 5–10 peaks/5 min (light gray), >10–100 peaks/5 min (gray), and >100 peaks/5 min (dark gray).

(K) Bar charts representing active cell number with mean ± SEM, proestrus inactive (N_{mice} = 9, 33 regions, n_{cells} = 2821), and proestrus active (N_{mice} = 8, 33 regions, n_{cells} = 2937; ***p < 0.0001), and corresponding LH serum measurements for proestrus inactive (N_{mice} = 9) and proestrus active (N_{mice} = 7, **p = 0.0015). Statistical analyses in (B), (C), (H), and K, unpaired t test (two-tailed). Experiments for (G)–(K) performed with $[K^+]_{ex}$ 8 mM.

A

0 mM [Ca²⁺]$_{ex}$

cell 1

cell 2

cell 3

$1 \, \Delta F/F_0$

1 min

B

n = 3 (245 cells)

**
Active cells [%]

1 mM   0 mM
[Ca²⁺]$_{ex}$

C

Cacna1c ⎤
Cacna1d ⎥ L-type
Cacna1f ⎦
Cacna1a — P/Q-type
Cacna1b — N-type
Cacna1g ⎤
Cacna1h ⎥ T-type
Cacna1i ⎦
Cacnb1 ⎤
Cacnb2 ⎥ Ca$_V$β
Cacnb3 ⎦
Cacna2d1 ⎤
Cacna2d2 ⎥ Ca$_V$α₂δ
Cacna2d3 ⎦

Juv ♂ Juv ♀ Adu ♂ Lac ♀ Di ♀ Pro ♀

Figure 2. Spontaneously active gonadotropes become silent in the absence of extracellular Ca²⁺

(A) [Ca²⁺]$_i$ activity in gonadotropes after the application of Ca²⁺-free ACSF solution. Cells 1 and 2 display spontaneous activity and initial [Ca²⁺]$_i$ increase upon application of Ca²⁺-free ACSF solution (indicated by black line). Spontaneous activity is blunted 1 min after solution exchange. Cell 3 represents a minority of cells, which display a [Ca²⁺]$_i$ increase in the absence of [Ca²⁺]$_{ex}$. $\Delta F/F_0$ is plotted versus time.

(B) Percentage active cells (active cell ≥5 peaks/ 5 min, **p = 0.0044) from three pituitaries. In total, 245 cells were compared using control measurements and measurements in Ca²⁺-free ACSF solution plotted as bar charts with means ± SEM. Statistical analysis, paired t test (two-tailed).

(C) VDCC subunit expression plotted using mean fragments per kilobase of exon per million mapped reads (FPKM) value. Values are standardized among six different hormonal stages (juvenile [Juv] males/ females, adult [Adu] males, lactating [Lac] females, diestrus [Di], and proestrus [Pro] females) and analyzed using the MATLAB clustergram script. Red, relatively high expression; blue, relatively low expression. The heatmap was generated using the transcriptome analysis from Qiao et al.[14]

oscillations in the absence of extracellular Ca²⁺ ([Ca²⁺]$_{ex}$). Most [Ca²⁺]$_i$ transients in gonadotropes within proestrus wholemount pituitaries were abolished by the exchange of 1 mM Ca²⁺ solution to Ca²⁺-free solution (Figures 2A and 2B). The mean percentage of active cells decreased from an average of 68.26% ± 6.02% to 2.67% ± 2.67% in Ca²⁺-free solution (N$_{mice}$ = 3, n$_{cells}$ = 245). After re-introducing external Ca²⁺ (1 mM), [Ca²⁺]$_i$ transients slowly reappeared with a delay of ~5 min. These data suggest that spontaneous [Ca²⁺]$_i$ activity in gonadotropes *in situ* results from Ca²⁺ entry across the plasma membrane and persists in the absence of the *in vivo* hormonal milieu, raising the possibility that the ion channel repertoire of gonadotropes changes throughout the estrous cycle.

Molecular modulation of gonadotropes at proestrus

Details about functional changes in gonadotropes on the molecular level during the altered endocrine conditions of different physiological states are just beginning to emerge. To address this question, we had previously produced enriched gonadotrope populations using fluorescence-activated cell sorting in order to perform mRNA sequencing.[14] When comparing the expression profile of murine gonadotropes at different hormonal stages, we found a high degree of molecular plasticity within these cells. Capitalizing on the RNA sequencing libraries, we found a striking plasticity of voltage-dependent Ca²⁺ channel (VDCC) subunit expression in gonadotropes that depend on the hormonal status of the animal. The majority of VDCC

and collected trunk blood for subsequent LH and FSH serum analysis (Figure S3). Importantly, every pituitary taken from animals in the LH surge featured spontaneously active gonadotropes. We also found spontaneous activity prior to the LH the surge (as evident by low LH and FSH serum levels). Interestingly, LH and FSH levels only from active pituitaries increased during the time course, being low prior to the surge and increasing during and at the end of the expected surge. Conversely, high serum FSH levels with accompanying low LH serum levels (as is typically found after the LH surge has passed) were largely restricted to pituitaries with less spontaneously active gonadotropes. Taken altogether, we speculate that the readily excitable state begins prior to—and is a prerequisite for—the LH surge.
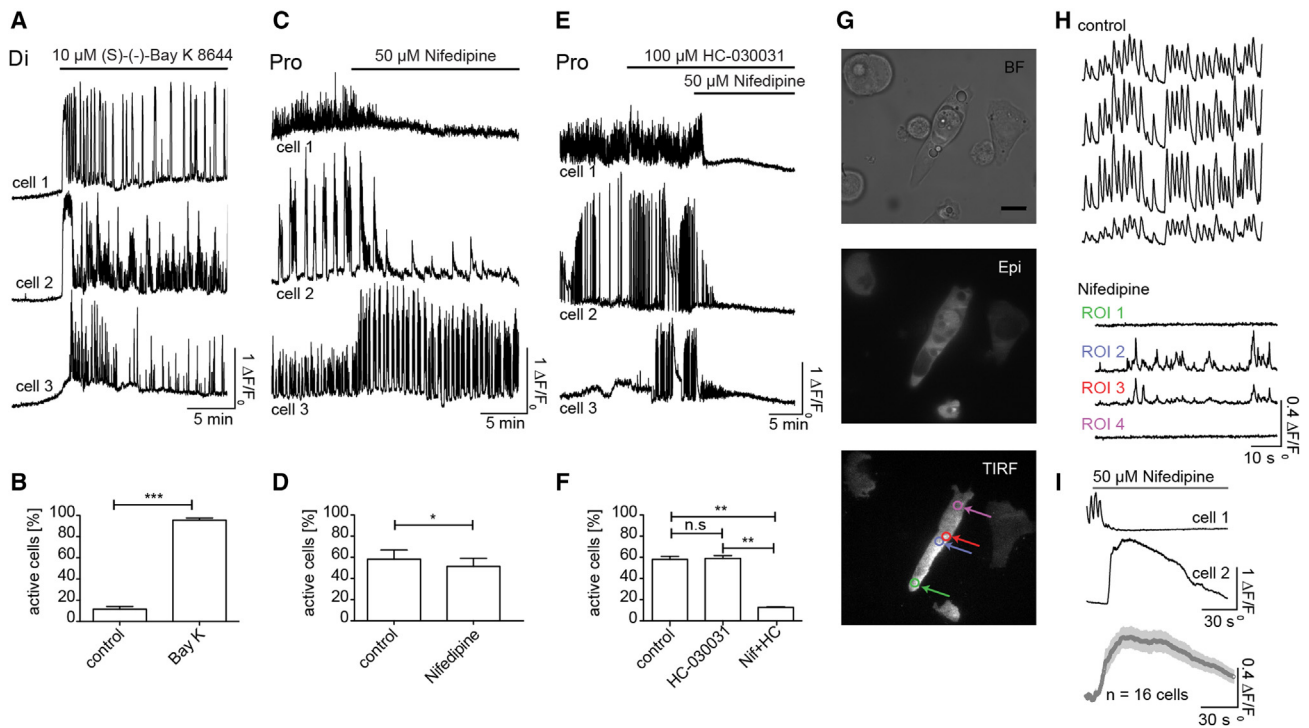
Preovulatory spontaneous [Ca²⁺]$_i$ activity in gonadotropes depends on [Ca²⁺]$_{ex}$

In order to test whether spontaneous [Ca²⁺]$_i$ transients in gonadotropes *in situ* depend on Ca²⁺ entry, we next characterized [Ca²⁺]$_i$

Figure 3. Pharmacological modulation of gonadotropes
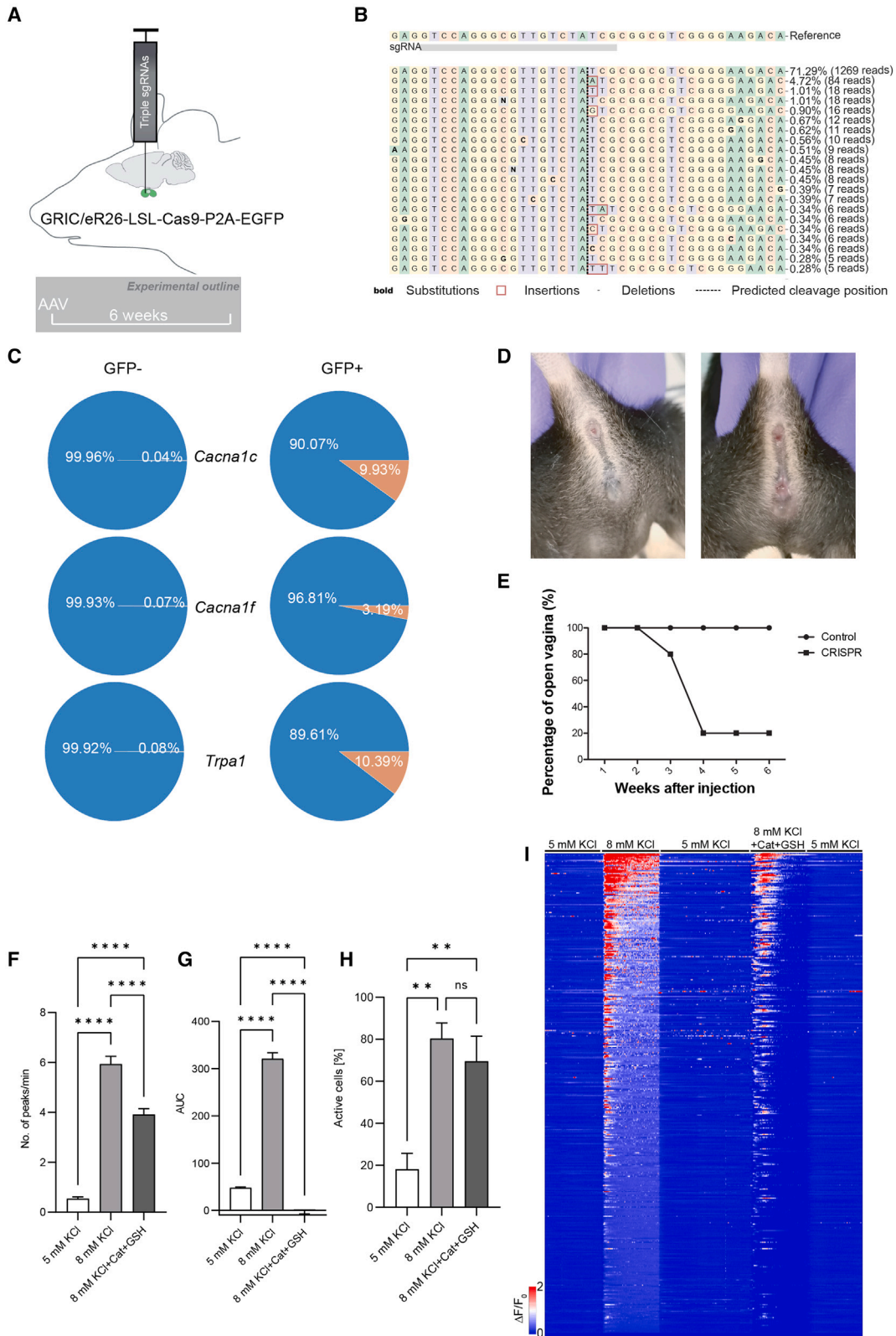
(A) Effect of L-type Ca^{2+}-channel agonist (S)-(−)-Bay K 8644 (10 μM) on silent diestrus gonadotropes (Di ♀, cells 1–3).

(B) Active gonadotrope percentage before ($N_{mice} = 3$, $n_{cells} = 286$) and during ($N_{mice} = 3$, $n_{cells} = 272$) 10- to 15-min Bay K application (***$p = 0.0003$).

(C) Representative $[Ca^{2+}]_i$ traces showing effect of nifedipine (50 μM).

(D) Spontaneously active gonadotrope percentage under control conditions ($N_{mice} = 3$, $n_{cells} = 257$) and in presence (10–15 min) of nifedipine ($N_{mice} = 3$, $n_{cells} = 268$; *$p = 0.0164$).

(E) Efficient block of $[Ca^{2+}]_i$ transients in gonadotropes by TRPA1 and L-type Ca^{2+}-channel blocker combination (100 μM HC-030031 and 50 μM nifedipine).

(F) Active gonadotrope percentage under control conditions ($N_{mice} = 3$, $n_{cells} = 241$), in presence (5–10 min) of HC-030031 ($N_{mice} = 3$, $n_{cells} = 241$), and in presence (10–15 min) of HC-030031 and nifedipine ($N_{mice} = 3$, $n_{cells} = 268$). Control vs. HC-030031, $p = 0.7225$; control vs. Nif + HC, **$p = 0.0058$; HC vs. Nif + HC, **$p = 0.0031$. Statistical analyses in (B), (D), and (F), paired t test (two-tailed); data are represented as mean ± SEM.

(G) Cultured pituitary cells in brightfield mode (BF; scale bar, 10 μm), GCaMP3-expressing gonadotropes under epifluorescence illumination (wavelength, 488 nm) and in total internal reflection fluorescence (TIRF) mode.

(H) Spontaneous $[Ca^{2+}]_i$ transients over time at different positions (regions of interest [ROIs] 1–4) of a gonadotrope cell under control and nifedipine (50 μM) blockage conditions. ROIs analyzed in (H) are color highlighted in (G) (TIRF).

(I) Single-cell $[Ca^{2+}]_i$ decrease (cell 1), increase (cell 2), and mean $[Ca^{2+}]_i$ increase profile ±SEM (16 cells) in gonadotropes upon nifedipine application. $\Delta F/F_0$ is plotted versus time.

subunits is specifically upregulated in the proestrus stage (Figure 2C). These data demonstrate cyclic molecular changes of the gonadotrope ion channel repertoire just before the LH surge. Taken together with the Ca^{2+} imaging data, these findings indicate that the transcriptional upregulation of VDCCs before ovulation leads to a cyclic functional gonadotrope modulation into a state of increased excitability to trigger ovulation.

Preovulatory spontaneous $[Ca^{2+}]_i$ activity in gonadotropes is ensured by L-type Ca^{2+} channels and TRPA1

We found that voltage-gated Ca^{2+} channels are enriched at proestrus, yet these channels are still expressed in diestrus. Therefore, it seems that the ion channel repertoire of gonadotropes at this stage might be insufficient to trigger spontaneous $[Ca^{2+}]_i$ transients despite the presence of some voltage-gated Ca^{2+}

channels. We therefore hypothesized that pharmacological activation of these channels might trigger $[Ca^{2+}]_i$ transients in silent gonadotropes. We tested this hypothesis by applying the L-type Ca^{2+}-channel agonist (S)-(−) Bay K 8644 (Bay K) to silent diestrus gonadotropes. Bay K application was indeed sufficient to induce $[Ca^{2+}]_i$ transients in almost all (95.58% ± 1.99%) diestrus gonadotropes (Figures 3A and 3B; control, $N_{mice} = 3$, $n_{cells} = 286$ vs. Bay K, $N_{mice} = 3$, $n_{cells} = 272$), demonstrating the presence of functional L-type Ca^{2+}-channels in these cells. We next tested the L-type Ca^{2+} channel blocker nifedipine (Nif) expecting to effectively silence active proestrus gonadotropes. Unexpectedly, however, gonadotrope responses to Nif were bimodal in whole-mount pituitary preparations (Figure 3C). Although some cells depicted the expected decrease in $[Ca^{2+}]_i$ (Figure 3C; cells 1 and 2), other gonadotropes responded instead with increased $[Ca^{2+}]_i$ signals (Figure 3C; cell 3). Overall, we only observed a small decrease in the percentage of spontaneously active

A

GRIC/eR26-LSL-Cas9-P2A-EGFP

Experimental outline

AAV — 6 weeks

B

bold Substitutions   ☐ Insertions   - Deletions   ------ Predicted cleavage position

C

GFP-   GFP+

Cacna1c   99.96%   0.04%   90.07%   9.93%

Cacna1f   99.93%   0.07%   96.81%   3.19%

Trpa1   99.92%   0.08%   89.61%   10.39%

D

E

Percentage of open vagina (%)

Weeks after injection

● Control
■ CRISPR

F   No. of peaks/min

G   AUC

H   Active cells [%]

5 mM KCl   8 mM KCl   8 mM KCl+Cat+GSH

I

5 mM KCl   8 mM KCl   5 mM KCl   8 mM KCl+Cat+GSH   5 mM KCl

$\Delta F/F_0$

(legend on next page)

gonadotropes in the presence of Nif (51.43%, N_{mice} = 3, n_{cells} = 268 vs. 58.27%, N_{mice} = 3, n_{cells} = 257 in controls; Figure 3D); suggesting that additional Ca^{2+} conductance might be involved in the generation of $[Ca^{2+}]_i$ transients in proestrus gonadotropes.

While Nif is a well-known L-type Ca^{2+} channel blocker, it is also a potent activator of TRP cation channels TRPA1 and TRPM3,[24,25] which also conduct Ca^{2+}. TRP channels play important functional roles in hormone-secreting cells, and we had previously shown that TRPA1 expression is specifically upregulated in proestrus gonadotropes.[14] In order to avoid Nif-dependent activation of TRPA1 channels in proestrus gonadotropes, we blocked TRPA1 using HC-030031 (HC) prior to Nif application. While pharmacological block of either L-type Ca^{2+} channels or TRPA1 failed to efficiently inhibit spontaneous gonadotrope activity (Figures 3E and 3F), the simultaneous block of both channels profoundly inhibited spontaneous activity in the majority (78%) of active proestrus gonadotropes (Figure 3F; percentage of active cells under control conditions, 58%, N_{mice} = 3, n_{cells} = 241 vs. 12.73%, N_{mice} = 3, n_{cells} = 268 in the presence of Nif + HC).

To visualize Ca^{2+} entry and spread within individual gonadotropes with higher resolution, we analyzed dissociated GCaMP3 gonadotropes with spontaneous activity prepared from adult females using total internal reflection fluorescence (TIRF) microscopy (Figure 3G). With this technique, we specifically visualize $[Ca^{2+}]_i$ within 230 nm of the plasma membrane on the side where the cells are attached to the substrate (i.e., at their footprint). Under control conditions, spontaneous Ca^{2+} signals spread homogeneously over the entire cell's footprint (Figure 3H). In the presence of Nif, overall Ca^{2+} entry was somewhat dampened and the spread of Ca^{2+} along the plasma membrane was strongly reduced (Figure 3H); however, Ca^{2+} entry was not completely abolished. Instead, we found discrete Ca^{2+} entry sites in some gonadotropes (19.35%, N_{mice} = 3, n_{cells} = 31) under L-type Ca^{2+} channel blockade. Furthermore, we observed a rise in $[Ca^{2+}]_i$ upon Nif application (Figure 3I, cell 2), rather than the expected decline (Figure 3I, cell 1), in 51.61%

of gonadotropes under these conditions. These data corroborate the whole-mount pituitary Ca^{2+} imaging results and show that Ca^{2+} entry in gonadotropes is mediated via additional Ca^{2+}-conducting channels such as TRPA1. Taken together, our findings demonstrate that both L-type Ca^{2+} channels and TRPA1 in the gonadotrope plasma membrane ensure the readily excitable state prior to ovulation.

Virus-assisted triple CRISPR-mediated knockout of *Cacna1c/Cacna1f/Trpa1* in gonadotropes disrupts reproductive function

To functionally analyze the role of L-type Ca^{2+} channels (encoded by *Cacna1c* and *Cacna1f*) and *Trpa1*, we used a CRISPR-Cas9 system to specifically disrupt the expression of these genes in the gonadotropes. We developed a mouse line, GRIC/eR26-LSL-Cas9-P2A-EGFP, which features Cas9 and GFP expression specifically in gonadotropes. Next, we stereotaxically injected an adeno-associated virus (AAV) to deliver guide RNAs targeting *Cacna1c*, *Cacna1f*, and *Trpa1* into the pituitary (Figure 4A). We originally sought to analyze the estrous cycle in these mice via vaginal cytology. Strikingly, however, even partial knockout of *Cacna1c*, *Cacna1f*, and *Trpa1* (Figures 4B and 4C) within the pituitary was sufficient to cause vaginal closure (Figures 4D and 4E) with LH and FSH serum levels comparable with inactive pituitaries (Figure S4). Taken together, these data demonstrate that *Cacna1c*, *Cacna1f*, and *Trpa1* are essential for normal gonadotrope physiology and that knockout of these genes even in only a fraction of the gonadotrope population is sufficient to abolish normal reproductive function.

Preovulatory hyperexcitability in gonadotropes requires ROS

Previous studies have shown that GnRH increases intracellular hydrogen peroxide levels in gonadotropes.[26,27] To gain mechanistic insight into the hyperexcitable state of the gonadotropes at proestrus, we investigated whether intracellular levels of

---

Figure 4. Virus-assisted triple Ca$_v$1.2, Ca$_v$1.4, and *Trpa1* knockout in gonadotropes leads to vaginal closure. Endogenous ROS is needed for preovulatory hyperexcitability of gonadotropes

(A) Illustration depicting stereotaxic delivery into mouse pituitary of an AAV encoding three guide RNAs (gRNAs) to concomitantly disrupt Ca$_v$1.2, Ca$_v$1.4, and *Trpa1* expression using CRISPR-Cas. AAVs were injected into GRIC/eR26-LSL-Cas9-P2A-EGFP mice (N_{mice} = 5), which express the Cas9 enzyme necessary for CRISPR-based knockout (KO) specifically in *Gnrhr*-expressing gonadotropes. The *Gnrhr*/Cas9 enzyme-expressing cells in these mice are also marked by EGFP. Control mice were produced by injection of AAV virus lacking any gRNAs into the same genotype (N_{mice} = 4).

(B) Distribution of identified *Trpa1* sequences around predicted CRISPR cleavage site from pituitary DNA of AAV5_triple gRNA-injected mouse, determined by CRISPResso2.

(C) Modified allele percentage (orange) from AAV5_triple gRNA-injected mouse in both GFP− cells (left) and GFP+ cells (right) for each of the three modified genes.

(D) Representative images of the vaginal closure phenotype observed in mice injected with the triple-gRNA AAV (left), compared with control-injected mice (right).

(E) Data from all mice depicting the vaginal closure over time following CRISPR-mediated KO of the three genes, compared with control mice.

(F) Number of Ca^{2+} peaks/min for gonadotropes from proestrus GRIC/eR26-GCaMP3 mice following application of 5 mM $[K^+]_{ex}$, 8 mM $[K^+]_{ex}$, or 8 mM $[K^+]_{ex}$ with catalase and glutathione (N_{mice} = 3, n_{cells} = 373, ****p < 0.0001).

(G) Area under the curve for Ca^{2+} responses following application of 5 mM $[K^+]_{ex}$, 8 mM $[K^+]_{ex}$, or 8 mM $[K^+]_{ex}$ with catalase and glutathione (N_{mice} = 3, n_{cells} = 373, ****p < 0.0001).

(H) Active cell percentage (≥5 peaks/5 min) following application of 5 mM $[K^+]_{ex}$, 8 mM $[K^+]_{ex}$, or 8 mM $[K^+]_{ex}$ with catalase and glutathione (N_{mice} = 3, n_{cells} = 373; 5 mM $[K^+]_{ex}$ vs. 8 mM $[K^+]_{ex}$, **p = 0.0048; 5 mM $[K^+]_{ex}$ vs. 8 mM $[K^+]_{ex}$ + Cat + GSH, **p = 0.0097; 8 mM $[K^+]_{ex}$ vs. 8 mM $[K^+]_{ex}$ + Cat + GSH, p = 0.502). Statistical analyses in (F), (G), and (H), one-way ANOVA. Bar charts are plotted as mean ± SEM.

(I) Heatmap of changes in normalized fluorescence intensities upon application of indicated solutions (373 cells pooled from three mice). Cells in the heatmap are represented in a descending order of fluorescence intensities of Ca^{2+} responses to 8 mM $[K^+]_{ex}$. Scale of fluorescence intensity changes in the heatmap are indicated by the color-coded bar.

ROS are crucial in this phenomenon. We measured $[Ca^{2+}]_i$ in gonadotropes from GRIC/eR26-GCaMP3 mice at proestrus, and observed that the hyperexcitability observed in response to 8 mM KCl application was significantly reduced in the presence of catalase and glutathione, which reduce intracellular ROS levels (Figures 4F and 4G). Interestingly, the number of peaks/min was reduced by 34% (Figure 4F; 8 mM KCl, 5.94 vs. 8 mM KCl + Cat + GSH, 3.92; N_{mice} = 3, n_{cells} = 373; p < 0.0001), while the area under curve was completely reduced (Figure 4G; 8 mM KCl, 320.99 vs. 8 mM KCl + Cat + GSH, −0.1; N_{mice} = 3, n_{cells} = 373; p < 0.0001). However, the percentage of active cells did not decrease significantly (Figure 4H; 8 mM KCl, 80.4% vs. 8 mM KCl + Cat + GSH, 69.53%; N_{mice} = 3, n_{cells} = 373; p = 0.502). Changes in fluorescence intensities upon the application of 8 mM KCl in the absence and presence of catalase and glutathione clearly demonstrate the contribution of endogenous ROS to the preovulatory hyperexcitability of gonadotropes (Figure 4I). These data indicate that intracellular signaling via ROS is at least partially responsible for the hyperexcitability observed in gonadotropes at proestrus.

DISCUSSION

Much research has focused on the regulation of LH and FSH release by neurons within the hypothalamus such as the GnRH neurons[28] and their afferents, the kisspeptin neurons.[14,29] Comparatively few studies, however, have asked whether the gonadotrope population itself is modulated to facilitate the changing requirements of the estrous cycle. Here, we find that the female gonadotrope population cyclically changes into an active stage persisting over many hours ex vivo in the absence of any hormonal or neuroendocrine stimulation. These data demonstrate that the gonadotrope population itself is molecularly tuned to meet the requirements of the specific reproductive cycle stage. Spontaneous $[Ca^{2+}]_i$ activity has also been reported in cultured rat gonadotropes isolated from ovariectomized females[30]; however, under these conditions, spontaneous activity did not seem to be related to LH release. In contrast, our data revealed a strong correlation between high LH serum levels and spontaneous activity within whole-mount pituitary preparations. Cultured cells are usually kept in medium for days before the Ca^{2+} imaging experiments with potential impact on gene expression and signaling. Moreover, ovariectomy affects gonadotrope function, since it changes the hormonal milieu by removing steroid hormone feedback to the pituitary and the hypothalamus.

We have previously shown that gonadotropes display unique transcriptome signatures not only during development but also in different stages of the reproductive cycle.[14] Here, we found that the majority of VDCC subunits were expressed at higher levels during proestrus. Changing the expression level of voltage-gated ion channels could feasibly augment the excitability of the gonadotropes, consistent with the state of hyperexcitability we detect at the time of the preovulatory LH surge. We further demonstrated that we could trigger $[Ca^{2+}]_i$ oscillations by pharmacologically activating L-type Ca^{2+} channels at diestrus, indicating a clear role for these channels in generating $[Ca^{2+}]_i$ transients in gonadotropes. Conversely, blockade of L-type Ca^{2+} channels alone was insufficient to abolish preovulatory

spontaneous $[Ca^{2+}]_i$ activity. Instead, blocking both L-type Ca^{2+} channels and TRPA1 was required to silence the gonadotropes, indicating mechanistic redundancy in order to ensure the change into a readily excitable state at the time of preovulatory LH surge. Interestingly, adding catalase and glutathione partially and completely reduced the number of peaks per minute and area under the curve, respectively, without decreasing the percentage of active cells. Thus, intracellular ROS, which are increased in gonadotropes by GnRH,[26,27] are partially responsible for the preovulatory hyperexcitability. In line with this, the gonadotropes remain active, albeit at a lower level, suggesting a complex interplay of multiple factors contributing to the observed hyperexcitability at proestrus. H_2O_2 activates both L-type Ca^{2+} channels and TRPA1.[31,32] TRPA1 has been well studied for its role as a cold sensor,[33] chemosensor,[34] and mechanosensory,[35] but little is known about the role of this ion channel in mammalian reproduction. Intriguingly, TRPA1 knockout mice have been described to have profound reproductive deficits[36]; however, the underlying mechanism has not yet been elucidated. Based on our data, it is tempting to speculate that preovulatory spontaneous $[Ca^{2+}]_i$ activity in gonadotropes might be disrupted in TRPA1 knockout mice. We propose that the preovulatory release of GnRH increases the intracellular ROS levels in gonadotropes via their proestrus-specific channel complement, activating the highly expressed L-type Ca^{2+} channels and TRPA1 and together manifesting the hyperexcitable phenotype observed at proestrus.

Taken together, our data demonstrate that, once per reproductive cycle, the gonadotrope population changes into a state of hyperexcitability. We show that this coincides with the LH surge and that this hyperexcitability is ensured by L-type Ca^{2+} channels, TRPA1, and ROS levels. We unequivocally demonstrate that L-type calcium channel subunits and TRPA1 within the gonadotropes are prerequisites for reproductive function in female mice and that modulation of ROS levels within the cell is a potential mechanism underlying this phenomenon. Importantly, our work demonstrates that gonadotropes not only respond to GnRH but undergo cycle-specific modulation of their channel complement in order to trigger ovulation via the LH surge.

Limitations of the study
While we demonstrate that ROS clearly plays an important role in gonadotrope hyperexcitability, we have not ruled out additional mechanisms contributing to this state. This study utilizes Ca^{2+} imaging in whole-mount pituitary preparations in order to dissect mechanisms behind the identified hyperexcitability state; however, emerging in vivo imaging technologies are expected to enable further refinement of our understanding of gonadotrope activity.

STAR★METHODS

Detailed methods are provided in the online version of this paper and include the following:

- KEY RESOURCES TABLE
- RESOURCE AVAILABILITY

SUPPLEMENTAL INFORMATION

Supplemental information can be found online at https://doi.org/10.1016/j.celrep.2023.112543.

AUTHOR CONTRIBUTIONS

U. Boehm, M.C., and V.G. conceived the study. V.G., S.Q., D.D., P.W., A.W., V.W., S.A., C.F.-T., M.R.M., I.G., K.K., and U. Becherer conducted experiments and analyzed data. P.L., P.M., R.R., and T.K. provided technical expertise and feedback. V.G., S.Q., M.C., D.D., A.W., and U. Boehm wrote the manuscript.

DECLARATION OF INTERESTS

The authors declare no competing interests.

REFERENCES

1. Fevold, H.L., Hisaw, F.L., and Leonard, S.L. (1931). The gonad stimulating and the luteinizing hormones of the anterior lobe of the hypophesis. Am. J. Physiol. *97*, 291–301. https://doi.org/10.1152/ajplegacy.1931.97.2.291.

2. Raj, H.G., and Moudgal, N.R. (1970). Effect of anti-luteinizing hormone serum on the ovulation of rats. Nature *227*, 1344–1345. https://doi.org/10.1038/2271344a0.

3. Childs, G.V. (2006). Chapter 29 - gonadotropes and lactotropes. In Knobil and Neill's Physiology of Reproduction, Third Edition, J.D. Neill, ed. (Academic Press), pp. 1483–1579. https://doi.org/10.1016/B978-012515400-0/50034-8.

4. Le Tissier, P., Campos, P., Lafont, C., Romanò, N., Hodson, D.J., and Mollard, P. (2017). An updated view of hypothalamic-vascular-pituitary unit function and plasticity. Nat. Rev. Endocrinol. *13*, 257–267. https://doi.org/10.1038/nrendo.2016.193.

5. Tse, A., and Hille, B. (1992). GnRH-induced Ca2+ oscillations and rhythmic hyperpolarizations of pituitary gonadotropes. Science *255*, 462–464. https://doi.org/10.1126/science.1734523.

6. Velardo, J.T. (1960). Induction of ovulation in immature hypophysectomized rats. Science *131*, 357–359. https://doi.org/10.1126/science.131.3397.357.

7. Cox, H.J. (1968). Length of menstrual cycle. Br. Med. J. *1*, 252–253. https://doi.org/10.1136/bmj.1.5586.252-b.

8. Allen, E. (1922). The oestrous cycle in the mouse. Am. J. Anat. *30*, 297–371. https://doi.org/10.1002/aja.1000300303.

9. Belchetz, P.E., Plant, T.M., Nakai, Y., Keogh, E.J., and Knobil, E. (1978). Hypophysial responses to continuous and intermittent delivery of hypopthalamic gonadotropin-releasing hormone. Science *202*, 631–633. https://doi.org/10.1126/science.100883.

10. Mortimer, C.H., Besser, G.M., Goldie, D.J., Hook, J., and McNeilly, A.S. (1973). Asynchronous changes in circulating LH and FSH after the gonadotrophin releasing hormone. Nat. New Biol. *246*, 22–23. https://doi.org/10.1038/newbio246022a0.

11. Sarkar, D.K., Chiappa, S.A., Fink, G., and Sherwood, N.M. (1976). Gonadotropin-releasing hormone surge in pro-oestrous rats. Nature *264*, 461–463. https://doi.org/10.1038/264461a0.

12. Knobil, E., Plant, T.M., Wildt, L., Belchetz, P.E., and Marshall, G. (1980). Control of the rhesus monkey menstrual cycle: permissive role of hypothalamic gonadotropin-releasing hormone. Science *207*, 1371–1373. https://doi.org/10.1126/science.6766566.

13. Beck, A., Götz, V., Qiao, S., Weissgerber, P., Flockerzi, V., Freichel, M., and Boehm, U. (2017). Functional characterization of transient receptor potential (TRP) channel C5 in female murine gonadotropes. Endocrinology *158*, 887–902. https://doi.org/10.1210/en.2016-1810.

14. Qiao, S., Nordström, K., Muijs, L., Gasparoni, G., Tierling, S., Krause, E., Walter, J., and Boehm, U. (2016). Molecular plasticity of male and female murine gonadotropes revealed by mRNA sequencing. Endocrinology *157*, 1082–1093. https://doi.org/10.1210/en.2015-1836.

15. Tse, A., Tse, F.W., and Hille, B. (1994). Calcium homeostasis in identified rat gonadotrophs. J. Physiol. *477*, 511–525. https://doi.org/10.1113/jphysiol.1994.sp020212.

16. Tse, F.W., Tse, A., Hille, B., Horstmann, H., and Almers, W. (1997). Local Ca2+ release from internal stores controls exocytosis in pituitary gonadotrophs. Neuron *18*, 121–132. https://doi.org/10.1016/s0896-6273(01)80051-9.

17. Zemkova, H., Kucka, M., Bjelobaba, I., Tomic, M., and Stojilkovic, S.S. (2013). Multiple cholinergic signaling pathways in pituitary gonadotrophs. Endocrinology *154*, 421–433. https://doi.org/10.1210/en.2012-1554.

18. Avelino-Cruz, J.E., Flores, A., Cebada, J., Mellon, P.L., Felix, R., and Monjaraz, E. (2009). Leptin increases L-type Ca2+ channel expression and GnRH-stimulated LH release in LbetaT2 gonadotropes. Mol. Cell. Endocrinol. *298*, 57–65. https://doi.org/10.1016/j.mce.2008.09.003.

19. Tsutsumi, R., Mistry, D., and Webster, N.J.G. (2010). Signaling responses to pulsatile gonadotropin-releasing hormone in LbetaT2 gonadotrope cells. J. Biol. Chem. *285*, 20262–20272. https://doi.org/10.1074/jbc.M110.132662.

20. Le Tissier, P.R., Hodson, D.J., Lafont, C., Fontanaud, P., Schaeffer, M., and Mollard, P. (2012). Anterior pituitary cell networks. Front. Neuroendocrinol. *33*, 252–266. https://doi.org/10.1016/j.yfrne.2012.08.002.

21. Wen, S., Schwarz, J.R., Niculescu, D., Dinu, C., Bauer, C.K., Hirdes, W., and Boehm, U. (2008). Functional characterization of genetically labeled gonadotropes. Endocrinology *149*, 2701–2711. https://doi.org/10.1210/en.2007-1502.

22. de Croft, S., Piet, R., Mayer, C., Mai, O., Boehm, U., and Herbison, A.E. (2012). Spontaneous kisspeptin neuron firing in the adult mouse reveals marked sex and brain region differences but no support for a direct role

in negative feedback. Endocrinology *153*, 5384–5393. https://doi.org/10.1210/en.2012-1616.

23. Murr, S.M., Geschwind, I.I., and Bradford, G.E. (1973). Plasma LH and FSH during different oestrous cycle conditions in mice. J. Reprod. Fertil. *32*, 221–230. https://doi.org/10.1530/jrf.0.0320221.

24. Fajardo, O., Meseguer, V., Belmonte, C., and Viana, F. (2008). TRPA1 channels: novel targets of 1,4-dihydropyridines. Channels *2*, 429–438. https://doi.org/10.4161/chan.2.6.7126.

25. Wagner, T.F.J., Loch, S., Lambert, S., Straub, I., Mannebach, S., Mathar, I., Düfer, M., Lis, A., Flockerzi, V., Philipp, S.E., and Oberwinkler, J. (2008). Transient receptor potential M3 channels are ionotropic steroid receptors in pancreatic beta cells. Nat. Cell Biol. *10*, 1421–1430. https://doi.org/10.1038/ncb1801.

26. Kim, T., and Lawson, M.A. (2015). GnRH regulates gonadotropin gene expression through NADPH/dual oxidase-derived reactive oxygen species. Endocrinology *156*, 2185–2199. https://doi.org/10.1210/en.2014-1709.

27. Dang, A.K., Chaplin, N.L., Murtazina, D.A., Boehm, U., Clay, C.M., and Amberg, G.C. (2018). Subplasmalemmal hydrogen peroxide triggers calcium influx in gonadotropes. J. Biol. Chem. *293*, 16028–16042. https://doi.org/10.1074/jbc.RA118.001830.

28. Campos, P., and Herbison, A.E. (2014). Optogenetic activation of GnRH neurons reveals minimal requirements for pulsatile luteinizing hormone secretion. Proc. Natl. Acad. Sci. USA *111*, 18387–18392. https://doi.org/10.1073/pnas.1415226112.

29. Han, S.Y., McLennan, T., Czieselsky, K., and Herbison, A.E. (2015). Selective optogenetic activation of arcuate kisspeptin neurons generates pulsatile luteinizing hormone secretion. Proc. Natl. Acad. Sci. USA *112*, 13109–13114. https://doi.org/10.1073/pnas.1512243112.

30. Iida, T., Stojilković, S.S., Izumi, S., and Catt, K.J. (1991). Spontaneous and agonist-induced calcium oscillations in pituitary gonadotrophs. Mol. Endocrinol. *5*, 949–958. https://doi.org/10.1210/mend-5-7-949.

31. Yang, L., Xu, J., Minobe, E., Yu, L., Feng, R., Kameyama, A., Yazawa, K., and Kameyama, M. (2013). Mechanisms underlying the modulation of L-type Ca^{2+} channel by hydrogen peroxide in Guinea pig ventricular myocytes. J. Physiol. Sci. *63*, 419–426. https://doi.org/10.1007/s12576-013-0279-2.

32. Trevisan, G., Hoffmeister, C., Rossato, M.F., Oliveira, S.M., Silva, M.A., Silva, C.R., Fusi, C., Tonello, R., Minocci, D., Guerra, G.P., et al. (2014). TRPA1 receptor stimulation by hydrogen peroxide is critical to trigger hyperalgesia and inflammation in a model of acute gout. Free Radic. Biol. Med. *72*, 200–209. https://doi.org/10.1016/j.freeradbiomed.2014.04.021.

33. Story, G.M., Peier, A.M., Reeve, A.J., Eid, S.R., Mosbacher, J., Hricik, T.R., Earley, T.J., Hergarden, A.C., Andersson, D.A., Hwang, S.W., et al. (2003). ANKTM1, a TRP-like channel expressed in nociceptive neurons, is acti-

34. Bautista, D.M., Jordt, S.E., Nikai, T., Tsuruda, P.R., Read, A.J., Poblete, J., Yamoah, E.N., Basbaum, A.I., and Julius, D. (2006). TRPA1 mediates the inflammatory actions of environmental irritants and proalgesic agents. Cell *124*, 1269–1282. https://doi.org/10.1016/j.cell.2006.02.023.

35. Corey, D.P., García-Añoveros, J., Holt, J.R., Kwan, K.Y., Lin, S.Y., Vollrath, M.A., Amalfitano, A., Cheung, E.L.M., Derfler, B.H., Duggan, A., et al. (2004). TRPA1 is a candidate for the mechanosensitive transduction channel of vertebrate hair cells. Nature *432*, 723–730. https://doi.org/10.1038/nature03066.

36. Tsuchiya, K., Kubota, K., Ohbuchi, K., Kaneko, A., Ohno, N., Mase, A., Matsushima, H., Yamamoto, M., Miyano, K., Uezono, Y., and Kono, T. (2016). Transient receptor potential ankyrin 1 agonists improve intestinal transit in a murine model of postoperative ileus. Neuro Gastroenterol. Motil. *28*, 1792–1805. https://doi.org/10.1111/nmo.12877.

37. Patel, T.P., Man, K., Firestein, B.L., and Meaney, D.F. (2015). Automated quantification of neuronal networks and single-cell calcium dynamics using calcium imaging. J. Neurosci. Methods *243*, 26–38. https://doi.org/10.1016/j.jneumeth.2015.01.020.

38. Paukert, M., Agarwal, A., Cha, J., Doze, V.A., Kang, J.U., and Bergles, D.E. (2014). Norepinephrine controls astroglial responsiveness to local circuit activity. Neuron *82*, 1263–1270. https://doi.org/10.1016/j.neuron.2014.04.038.

39. Labun, K., Montague, T.G., Krause, M., Torres Cleuren, Y.N., Tjeldnes, H., and Valen, E. (2019). CHOPCHOP v3: expanding the CRISPR web toolbox beyond genome editing. Nucleic Acids Res. *47*, W171–W174. https://doi.org/10.1093/nar/gkz365.

40. Bae, S., Park, J., and Kim, J.S. (2014). Cas-OFFinder: a fast and versatile algorithm that searches for potential off-target sites of Cas9 RNA-guided endonucleases. Bioinformatics *30*, 1473–1475. https://doi.org/10.1093/bioinformatics/btu048.

41. Hellier, V., Brock, O., Candlish, M., Desroziers, E., Aoki, M., Mayer, C., Piet, R., Herbison, A., Colledge, W.H., Prévot, V., et al. (2018). Female sexual behavior in mice is controlled by kisspeptin neurons. Nat. Commun. *9*, 400. https://doi.org/10.1038/s41467-017-02797-2.

42. Clement, K., Rees, H., Canver, M.C., Gehrke, J.M., Farouni, R., Hsu, J.Y., Cole, M.A., Liu, D.R., Joung, J.K., Bauer, D.E., and Pinello, L. (2019). CRISPResso2 provides accurate and rapid genome editing sequence analysis. Nat. Biotechnol. *37*, 224–226. https://doi.org/10.1038/s41587-019-0032-3.

43. Caligioni, C.S. (2009). Assessing reproductive status/stages in mice. Curr. Protoc. Neurosci. *48*, A.4I.1–A.4I.8. https://doi.org/10.1002/0471142301.nsa04is48.

vated by cold temperatures. Cell *112*, 819–829. https://doi.org/10.1016/s0092-8674(03)00158-2.

STAR★METHODS

KEY RESOURCES TABLE

REAGENT or RESOURCE	SOURCE	IDENTIFIER
Bacterial and virus strains		
AAV5-U6-*Cacna1f/Trpa1/Cacna1c*-CAG-mCherry	This paper	N/A
AAV5-U6-control-CAG-mCherry	This paper	N/A
Chemicals, peptides, and recombinant proteins		
(S)-(−)-Bay K 8644	Tocris	Cat#1546
Nifedipine	Sigma	Cat#N7634
HC-030031	Alomone Labs	Cat#H-105
Critical commercial assays		
MILLIPLEX Map Mouse Pituitary Magnetic Bead Panel	Merck	Cat#MPTMAG-49K
HEPES	Sigma	Cat#H3375
$MgCl_2 \cdot 6xH_2O$	Sigma	Cat#M2670
NaCl	Grüssing Gmbh	Cat#121221000U
KCl	Roth	Cat#6781.1
$CaCl_2 \cdot 2xH_2O$	Sigma	Cat#C3306
$NaHCO_3$	Roth	Cat#6885.1
NaH_2PO_4	Roth	Cat#4984.1
D-(+)-Glucose	Roth	Cat#X997.2
EGTA	Roth	Cat#3054.3
BSA	Sigma	Cat#A2153
EDTA	Sigma	Cat#ED2SC
Papain dissociation system	Worthington	Cat#LK003150
L-Glutathione Reduced	Sigma	Cat#G4251
Catalase	Sigma	Cat#C9322
Experimental models: Organisms/strains		
Mouse: GnRHR-IRES-Cre (GRIC)	(Wen et al.)[21]	N/A
Mouse: eR26-GCaMP3	The Jackson Laboratory	Jackson strain number 028764
Mouse: eR26-LSL-Cas9-P2A-EGFP	The Jackson Laboratory	Jackson strain number 024857
Software and algorithms		
FluoroSNNAP (Fluorescence Single Neuron and Network Analysis Package) tool for MATLAB	(Patel et al.)[37]	https://github.com/tapan-patel/FluoroSNNAP
Automated peak counting using MATLAB	MathWorks	https://www.mathworks.com/
Prism	GraphPad	https://www.graphpad.com/
Oligonucleotides		
Cacna1c forward: GGACAGCAGGGGTGAGACAA	This paper	N/A
Cacna1c reverse: GCGTCATGCCTGGTGAAAGG	This paper	N/A
Cacna1f forward: AGCTTCAGAGTGGCAGGGAC	This paper	N/A
Cacna1f reverse: CCATGGCATCCTGCATCTGG	This paper	N/A
Trpa1 forward: GCTTAGTTGTAGGTCCCAAGTCC	This paper	N/A
Trpa1 reverse: GGTGCTGTGTACCCTGATACTG	This paper	N/A
Other		
Cacna1c guideRNA: GTTATCGAACGTGCTCCTAC	This paper	N/A
Cacna1f guideRNA: GAAGTTCGTGATGCCACCGT	This paper	N/A
Trpa1 guideRNA: GTCCAGGGCGTTGTCTATCG	This paper	N/A

RESOURCE AVAILABILITY

Lead contact
Further information and requests for resources and reagents should be directed to and will be fulfilled by the Lead Contact, Ulrich Boehm (ulrich.boehm@uks.eu).

Materials availability
AAVs generated in this study will be made available by the lead contact upon reasonable request.

Data and code availability
- All data reported in this paper will be shared by the lead contact upon request.
- This paper does not report original code.
- Any additional information required to reanalyze the data reported in this paper is available from the lead contact upon request.

EXPERIMENTAL MODEL AND SUBJECT PARTICIPANT DETAILS

Mice
Animal care and experimental procedures were approved by the animal welfare committee of Saarland University and were performed in accordance with their established guidelines. Experiments were designed based on accepted standards of animal care and all efforts were made to minimize animal suffering. Mice were kept under a standard light/dark cycle with food and water *ad libitum*. GnRHR-IRES-Cre (GRIC) knock-in mice coexpress the GNRHR with Cre-recombinase.[21] The eR26-GCaMP3 reporter line (Jackson strain number 028764) carries a Cre-activated GCaMP3 under the control of the enhanced *ROSA26* locus.[38] Heterozygous GRIC/eR26-GCaMP3 animals in different developmental and hormonal stages were used. The eR26-LSL-Cas9-P2A-EGFP line carries a Cre-activated Cas9 gene and GFP under the control of the enhanced ROSA26 locus (Jackson strain number 024857). Adult female heterozygous GRIC/eR26-LSL-Cas9-P2A-EGFP animals were used for stereotactic injections of AAVs carrying multiple specific guide RNAs into the pituitary to achieve cell-specific gene knockouts.

METHOD DETAILS

Cloning and guide RNA selection
Potential guide RNA (gRNA) sequences were identified using Chopchop[39] for each of the 3 genes (*Cacna1c*, *Cacna1f* and *Trpa1*). From the generated gRNA sequences, an optimal gRNA was selected using both Chopchop and a second program; CasOFFfinder,[40] such that minimal potential off-target binding sites existed. The following gRNAs were selected for targeting; *Cacna1c*: GTTATCGAACGTGCTCCTAC; *Cacna1f*: GAAGTTCGTGATGCCACCGT and *Trpa1*: GTCCAGGGCGTTGTCTATCG. Each gRNA was generated as a primer dimer and then independently cloned into either px330A-1x3 (Addgene plasmid no. 58767), px330S-2 (Addgene plasmid no. 58778) or px330S-3 (Addgene plasmid no. 58779) using the *BbsI* sites present in each of these plasmids. This inserted each gRNA sequence subsequent to a U6 promoter and immediately upstream of the gRNA scaffold sequence required for correct interaction with the Cas9 protein. Following sequence verification, the 3 U6/gRNA/scaffold constructs were cloned such that they were all present sequentially in the same plasmid using a Gateway cloning strategy in conjuction with the *BsaI* restriction enzyme. Subsequently, the *MluI* recognition sequence was cloned into AAV5-U6-control-CAG-mCherry (Addgene plasmid no. 91947) and this site was used alongside *Acc65I* to ligate the entire block containing the 3 U6/gRNA/scaffold into the mCherry-containing plasmid, generating AAV5-U6-*Cacna1f*/*Trpa1*/*Cacna1c*-CAG-mCherry (triple gRNA plasmid). The correct incorporation of all elements was verified by sequencing of the entire region contained between the 2 ITR sites. For production of a control virus, the unmodified AAV5-U6-control-CAG-mCherry (Addgene plasmid no. 91947) was used. Sequences of the plasmids used to generate both experimental and control AAVs are identical in all aspects except that no gRNA sequences are present in the control plasmid.

AAV vector production
Both the triple gRNA and control viruses were produced using the triple transfection helper-free method. This involved transfecting HEK293T cells in culture with 3 plasmids in a 1:1:1 ratio, the first containing viral genes such as E2 and E4 (phelper Addgene plasmid no. 112867), the second which facilitates generation of serotype 5 AAV vectors (pAAV2/5 – Addgene plasmid no. 104964) and the third which dictates the packaged contents of the virus particles, namely either the triple gRNA plasmid (to generate the triple gRNA AAV) or control plasmid (for control AAV generation) previously described under "cloning and guide RNA selection." Transfection was undertaken when the cells reached 60–70% confluence using a 4:1 (v:w) ratio of Polyethylenimine (PEI) to plasmid DNA. 60–72 h after transfection, cells were pelleted and processed to recover the virus. Virus samples were then subjected to purification through an Iodixanol gradient before desalting and concentration using a centrifugal filter (MWCO 100). Viral titer was measured by qPCR analysis with primers specific to the ITR region of the packaging plasmid.

Stereotaxic injection

Stereotaxic injections were performed as follows: six injections with 0.5μL per injection of either triple gRNA AAV or control AAV were injected to the pituitary. Coordinates were −2.55 mm, −2.7 mm and −2.95 mm antero-posterior, ±0.6 mm lateral to midline, 300 μm above the *sella turcica*.[41] Animals were checked for vaginal opening every day for 6 weeks.

CRISPR efficiency verification

6 weeks after AAV injection, pituitaries were removed from the mice. Pituitaries were then dissociated using papain and deoxyribonuclease in Earle's balanced salt solution (Papain dissociation system; Worthington), and gently agitated for 30 min at 37°C.[13,14] The tissue was then mechanically dissociated by pipetting repeatedly with a fire-polished glass pipette. The dissociated cells were transferred to a 15-mL tube and centrifuged for 5 min at 2500 rpm. Then, the supernatant was discarded and the pellet was resuspended in 1 mL FACS buffer (0.1% BSA and 1% EDTA in PBS). GFP positive pituitary cells were sorted by using SH800S Cell Sorter. GFP negative cells were used as control. The dissociated cells were sorted by fluorescence (endogenously expressed GFP) with excitation at 488 nm and emission detected at 508 nm. Approximately 20000 sorted cells were obtained for each condition. DNA was extracted from sorted cells and then targeted amplification was performed via PCR with the primers against *Cacna1c, Cacna1f* or *Trpa1* (*Cacna1c* forward: GGACAGCAGGGGTGAGACAA, *Cacna1c* reverse: GCGTCATGCCTGGTGAAAGG; *Cacna1f* forward: AGCTTCAGAGTGGCAGGGAC, *Cacna1f* reverse: CCATGGCATCCTGCATCTGG; *Trpa1* forward: GCTTAGTTG TAGGTCCCAAGTCC, *Trpa1* reverse: GGTGCTGTGTACCCTGATACTG). Amplicons were generated using the above region-specific primers with additional Illumina universal adaptor sequences. PCR products containing adaptors were purified with Agencourt AmpureBeads and indexed in a second PCR using Illumina TruSeq adapters. After final AmpureBead Purification amplicons were pooled in an equimolar ratio and sequenced on a MiSeq (Illumina) using the MiSeq Reagent Kit v2 (500-cycles) in paired-end mode, aiming at 10,000 reads per amplicon. The sequence was then analyzed by CRISPResso2.[42]

TIRF microscopy

Images were acquired using an inverted IX 70 microscope (Olympus) equipped with a 100 x/1.45 NA Plan Apochromat Olympus objective, a TILL-TIRF condenser (TILLPhotonics), and an Evolve512 EMCCD camera (Photometrics). The final pixel size was 160 nm.

Vaginal cytology

Estrous cycle stages were determined by daily vaginal cytology; the vagina was flushed 3–5 times with approximately 10 μL PBS and unstained samples were smeared on a glass slide and observed under a light microscope with 10x objective (Imager.M2, Zeiss).[43] The 4 main estrous cycle stages (proestrus (1), estrus (2), metestrus (3), diestrus (4)) were further divided and intermediate stages such as late proestrus (1.5), late estrus (2.5), late metestrus (3.5) and late diestrus (4.5), were introduced to predict the estrous cycle stage more accurately (Figure S1). Before Ca^{2+} imaging, females went through at least three consecutive cycles. Proestrus females were sacrificed between 4.5 and 0.5 h before the night phase, corresponding to the proestrus LH surge.[22] Diestrus females were sacrificed during the mid-light phase. All other animals at the developmental stages mentioned above were sacrificed during the light-phase.

Ca^{2+} imaging

GRIC/eR26-GCaMP3 animals in different hormonal stages were decapitated and the pituitary quickly removed and transferred into ice-cold carbogenated artificial cerebrospinal fluid (ACSF 1) (containing (in mM) 124 NaCl, 5 KCl, 2 $CaCl_2$, 1 $MgCl_2$, 25 $NaHCO_3$, 1.25 NaH_2PO_4, 5 glucose, pH ~7.4 RT, osmolality ~300 mosmol/kg) or ACSF 2 for spontaneous Ca^{2+} imaging recordings, (containing (in mM) 124 NaCl, 8 KCl, 1 $CaCl_2$, 0.8 $MgCl_2$, 25 $NaHCO_3$, 1.25 NaH_2PO_4, 5 glucose). The whole pituitary was placed into the recording chamber (Warner Instruments, RC-27LD) with the ventral side up and surrounded by 4% low melting point agarose (Thermo Scientific). Solutions (ACSF, nifedipine, (S)-(−)-Bay K 8644, HC-030031) and the chamber were continuously heated to 37°C (Warner Instruments, dual automatic temperature controller) resulting in a bath solution of ~33°C. The whole-mount pituitary was allowed to recover and adapt to the preheated chamber for 30 min before the recordings were performed. All solutions were bath-applied at a flow rate of 2 mL/min (Warner Instruments, VC-6 Valve Controller). Ca^{2+} imaging experiments were performed using an upright confocal microscope (Zeiss, LSM 710), excitation light 488 nm (argon laser) and emission filter at 493–598 nm. Images (512 x 512 pixel) were taken with a frame rate of 2 Hz using a water immersion 20 x/1.0 NA objective (Zeiss, Plan-Apochromat). Nifedipine (50 μM, Sigma-Aldrich, N7634) and (S)-(−)-Bay K 8644 (10 μM, Tocris, 1546) were applied for 20 min after a control measurement (5–10 min). TRPA1 activation was blocked for 10 min using HC-030031 (100 μM, Alomone Labs, #H-105) followed by a 20-min application of both blockers, HC-030031 and nifedipine. At the end of the experiment high K^+ solution was administered as a control for cell viability. For ROS-scavenging experiments, 5 mM and 8 mM $[K^+]_{ex}$ were applied for 5 min each, followed by washing with 5 mM $[K^+]_{ex}$ for 8 min; 8 mM $[K^+]_{ex}$ with catalase (2000 U/ml, Sigma, C9322) and glutathione (1 mM, Sigma, G4251) was then applied for 5 min, followed by a 5-min wash with 5 mM $[K^+]_{ex}$.

Hormone measurements

Trunk blood was collected from mice just before the Ca^{2+} imaging experiment and allowed to clot for 30 min at room temperature, centrifuged (Centrifuge 5418R) for 10 min at 4 °C at 2,000xg, the serum removed and subsequently centrifuged for a further 10 min at 4 °C at 2,000xg. The serum was then transferred to a fresh tube for storage at −20°C until needed. Hormone measurements were performed using the Luminex xMAP technology (MAGPIX, Luminex Corporation) in combination with the mouse pituitary kit (MPTMAG-49K, Merck Millipore) according to the manufacturer's instructions. In brief, the 96-well plate was loaded with one background sample, standard 1 to 7 samples, and 2 quality control samples, followed by the actual biological serum samples (up to 38 samples, each sample was pipetted twice). Different antibody-immobilized beads were added into each well and incubated over night at 4°C. Wells were washed the next day and incubated in biotinylated antibodies at room temperature followed by additional incubation with Streptavidin-Phycoerythrin (PE). Hormone measurements were performed using a MAGPIX Luminex machine (Luminex Corporation). The excitation via the red LED serves for bead detection based on their emission wavelength. The excitation with the green LED determines the magnitude of the bound antigen based on emission intensity. The analysis was performed using the xPONENT software. The mean was calculated for the duplicates and all measurements with an intra-assay value above 20% were excluded. Standard curves were generated using the best fit option in xPONENT (Luminex Corporation) resulting in standard curves fitted mainly to the 5 parameters linear scale weighted model with a coefficient of determination R^2 between 0.998 and 1. In four independent runs the quality controls were within 97% of the expected range with the remaining 3% below the minimum expected value. Using the quality controls from these 4 independent runs, the inter-assay CV% was calculated to be 19.7%.

QUANTIFICATION AND STATISTICAL ANALYSIS

Analyses of Ca^{2+} signals in whole-mount pituitaries

ROIs were manually marked using the FluoroSNNAP (Fluorescence Single Neuron and Network Analysis Package) tool for MATLAB.[37] In order to analyze spontaneous $[Ca^{2+}]_i$ spikes in gonadotropes isolated at different hormonal stages, active cells were initially quantified manually. 3 pituitary regions were chosen from 3 different pituitaries isolated from proestrus females with gonadotropes showing spontaneous Ca^{2+} signals. Each region was analyzed manually by counting the percentage of cells exhibiting spontaneous Ca^{2+} signals. Next the number of Ca^{2+} peaks was quantified per cell and per region. These manually acquired data were then used to establish a method to automate peak counting using MATLAB. As shown in Figure S2A the method using the slope ($\Delta F/F_{0slope}$) of the baseline-corrected $[Ca^{2+}]_i$ signals ($\Delta F/F_0$) and the counting of spikes above the threshold of 0.15 $\Delta F/F_{0slope}$ correlated well with the manually acquired peak counts (Figure S2B). The number of $[Ca^{2+}]_i$ peaks obtained by manual vs. automated counting were not significantly different (Figure S2C), validating the parameters used for peak detection. Additionally, we calculated the percentage of cells per pituitary region and compared these values to the automated ones. Cells with a minimum detected peak number of 5/5 min were defined as active cells. When comparing to the automated method, with regard to the percentage of active cells, we found an acceptable difference of 13 ± 4.5% to the manually acquired percentage. Manual counting is generally time consuming and might evoke bias. In addition, it appeared to be difficult or almost impossible to determine the number of peaks in about 27% of cells (total cell no. = 241) due to poor signal-to-noise ratio (Figure S2A) or wave-like $[Ca^{2+}]_i$ signals without any particular peak. Therefore, the automated method of cell counting with the above-mentioned threshold was applied to all measurements in order to compare spontaneous $[Ca^{2+}]_i$ activity of gonadotropes between different hormonal stages. Pharmacological activation/silencing of gonadotropes was manually analyzed comparing the percentage of active cells within a time window of 5 min before and after agonist/antagonist application. Heatmaps for the fluorescence responses were made using MATLAB.

Statistics and illustrations

Unpaired t test (two-tailed), paired t test (two-tailed), one-way ANOVA and two-tailed Mann-Whitney test were used as detailed in the figure legends. All statistical analyses and the generation of graphs were performed using GraphPad software and R. Figures were prepared using ZenBlack, Fiji, Adobe Illustrator and Photoshop, Affinity Designer, Affinity Photo and Blender.